Research Article

Effect of transient temperature on 304 stainless steel LPG tank structure using numerical simulation approach

Chukwugozie Jekwu Ejeh[1] · **Gbemisola Precious Akhabue**[2] · **Isaac Agyeibi**[1]

Received: 23 September 2019 / Accepted: 21 November 2019 / Published online: 26 November 2019

Abstract
The use of numerical simulation approach to investigate the effect of transient boundary temperature on an LPG tank structure was investigated. Here, both transient thermal and structural system were coupled in ANSYS software version 19.2 to create an interaction between the thermal and mechanical load on the tank structure. The focus of this paper is to identify stress hotspot which may eventually lead to stress-corrosion using a non-linear solver. Literature has proven that temperature gradient acting on a material is a possible cause for failure in most engineering structures due to stress induced corrosion. In this study the effect of a time dependent change in the temperature of the material (304 stainless steel) was investigated. The temperature was set to increase from cryogenic to 30 °C, and the pressure which represents mechanical load was also implemented at the wall boundary. Results obtained showed that stress was concentrated at the principal plane connecting the tank roof to the cylindrical structure. However, a failure analysis was conducted were the mechanical load was increased to 3×10^{43} Pa. It was found that the material failed after 1,000,000 s time steps and the tensile yield strength obtained from the stress–strain curve was lower than the material standard value. This can be explained with the concept that the action of temperature disrupted the material microstructure, hence, reduced the material stiffness to fracture. The stress–strain curve was validated with the standard plot for the 304 stainless steel material type.

Keywords Failure analysis · Stainless steel · LPG storage tank · Extreme temperatures · Transient thermal analysis · Transient structural analysis

1 Introduction

The application of 304 stainless steel materials in recent years for the construction of engineering structures are of increasing demand in the industry [2, 5]. Carbon steel materials being harder, good heat distributor and easy to sharpen compared to stainless steel is less preferred for use to build pipelines, metallic implants, bridges, storage vessels, offshore platforms and many more. The wide application of 304 stainless steel materials is derived from its corrosion, chemical resistance and the ability to prevent stain from contaminants in its surrounding [4]. Therefore making 304 more preferred than carbon steel.

In this paper, a typical liquefied petroleum gas (LPG) vertical storage tank made from a 304 stainless steel material was used for the analysis. LPG is a type of gaseous hydrocarbon liquefied at room temperature and pressure of magnitude 101,425 Pa for use in cooking, heating homes and as fuel source [15]. It is mainly composed of propane and butane at a specified proportion [17]. In The United Kingdom, LPG is obtained from 100% propane and are classified as Grade A.

✉ Chukwugozie Jekwu Ejeh, echukwugozie@gmail.com; Gbemisola Precious Akhabue, gbemisolaakhabue1@gmail.com; Isaac Agyeibi, iagyeibi@aanuc.edu.gh | [1]All Nations University College, P.O Box KF 1908, Koforidua, Eastern Region, Ghana. [2]Presbyterian University College, Akropong, Ghana.

Studies has proven that the thermodynamic property of the fluid is greatly influenced by temperature and pressure from the surrounding. Examples includes boiling point, thermal expansion, and vapor pressure. The action of pressure and temperature gradient on the fluid, causes work to be done and therefore contributes in increasing the internal energy of the system. From the real gas theory, the gas molecules moves randomly in a container and collides in-elastically with the wall of the container thereafter. The intensity of the molecular vibration is directly linked to the amount of thermal energy absorbed by the fluid. The rise in the vibrational frequency of the gas molecules is sourced from heat transfered from the surroundings and mechanical work done on the system. The result of the gas–wall interaction transfer momentum energy to the material microstructure. Hence, stress is generated on the material and could eventually contribute to failure at the long run.

The American Society of Metals postulates that the 304 stainless steel material will deform at a load of 213 MPa. Most a times, the load acting on LPG storage tanks in the refinery or processing plant could exceed this theoretical limit at a pro-long time interval, and could cause the material to experience fatigue stress and eventually fail or collapse [9, 13].

Thermal load resulting from heat action was found to be a common cause for stress concentration and failure of structures built from a 304 stainless steel material. Adnyana [3] recently conducted an interesting research concerned with the failure analysis of stainless steel heat exchanger tubes for use in a petrochemical plant, published with the Journal of Failure Analysis and Prevention. He investigated on a case where the shell and tube of the heat exchanger failed after a year of maintenance work. Metallurgical examination, chemical analysis, hardness testing and microscopic examination approaches were carried out by Adnyana [3] to identify the cause of failure. However, his study informed that the heat exchanger tubes exposed to high heat levels failed due to stress-corrosion cracking. The thermal stress exerted on the material was as a result of the consistent change in the temperature gradient at local points. Furthermore, Maharaj and Marquez [12] looked into the failure of a stainless steel pipe elbow used in the transportation of purge gas. The material type was an SA-312 TP04 stainless steel. It was found that the material failed due to local stress at the welded points, and can be accounted by the extreme steady-state piping vibration at welded points were the thermal stress was experienced. The microstructural and vibrational evaluation techniques were implemented for the evaluation for the possible cause of failure.

Kumar et al. [11] also investigated on the failure analysis of stainless steel pipes for use in the petrochemical industry. In his investigation, hydrogen was transmitted through the pipeline to a reactor. Leak points were identified on the pipe surface. Reactors emits high levels of heat energy, as a result the transmission pipes were exposed to the heat intensity. From his findings, the action of heat on the material had an influence on the pipe structural integrity. Specific areas were observed to have experienced local rise in temperature gradient and caused stress to be generated. As a result, the pipe surface was found to corrode due to local stress.

Fuller et al. [7] demonstrated that the failure analysis of an AISI 304 stainless steel shaft can be achieved using the conventional 14-step failure analysis approach. The approach involves mechanical testing, nondestructive testing, metallography, chemical analysis, but does not include detail transient thermal analysis coupled with the model structure. This study showed that the steel shaft failed at specific areas due to intergranullar stress cracking. The failure rate was rapid at heat affected zones.

Furthermore, Reinders et al. [15] investigated on the effect of pressure and temperature increase of LPG stored in a thermally coated pressure vessel exposed to surrounding fire out break from the boiling liquid expanding vapour explosion (BLEVE), using experimental approach. The environment temperature of the LPG tank was varied from cryogenic in LNG-tanks to over 1000 °C in a fire. The results obtained showed that extreme temperatures was the main cause why the tank structure behaviour deviated from normal. However, a 2-D Computational Fluid Dynamics (CFD) approach was used by Scarponi et al. [16] to study the behaviour of LPG tanks exposed to wild-land fires and, similar conclusion with Reinders et al. [15] work was made.

Critical review of the literature therefore informs that, heat has a negative impact on stainless steel material modulus of elasticity, as a result, it is possible that tools and structures made from stainless steel materials could fail due to heat induced stress. This forms the basis for our investigation were we seek to identify regions exposed to intense heat from the surrounding condition and, estimate the stress induced by the heat action on the material using a numerical approach. The numerical simulation approach involves coupling both thermal and structural system in ANSYS software, to model thermal and structural interaction. Here, a vertical LPG storage tank is used as the case structure for the investigation.

Despite the extensive studies on the failure analysis of stainless steel materials from literature, the application of a coupled transient thermal and structural system approach is rare in literature. Therefore, this paper focuses on performing failure analysis on a typical LPG storage tank model made from a stainless steel material under the influence of transient thermal and mechanical

load. The study is subdivided into two specific objective. The first is to identify areas with the potential for failure under a relatively low temperature range, and to further perform failure analysis on the structure under a relatively high static temperatures and pressure. The two key measurable parameters for this study are the Von Misses stress, and Total Mechanical and Thermal equivalent strain.

2 Methodology

2.1 Simulation approach

This section focuses on describing the numerical simulation approach employed to achieve the set objectves. As mentioned previously in the introduction section, ANSYS structural coupled with the Transient thermal system was used for the simulation. The methodology flow chart or algorithm employed can be seen in Fig. 1 below. The data used to create the model geometry were hypothetical. The fluid and tank material information were obtained from ANSYS engineering data library for analytic purpose. It was made freely available and correlated well with standard values. The LPG (propane) and stainless steel material data are shown in the Tables 1 and 2, respectively.

The model geometry was created using the ANSYS Geomodeler. The model geometry comprises of Four (4) different part, namely, the tank roof, cylindrical body, bottom support and the fluid domain. Figure 2a, b shows the tank model and a sketch describing the dimensions of each design considerations. Further details on the design parameters are provided in Table 3. The tank roof was designed from two (2) arcs of length 67.3 m (major arc) and 65.9 m (minor arc) and rotated 180° through the vertical axis to form a semi elliptical shape of thickness 1.4 m. It was further revolved 360° with reference to the vertical axis (y-axis) to form a solid figure. The cylindrical part of the tank was designed from a rectangular sketch of height and thickness 24.4 m and 2.3 m respectively. It was then revolved 360° through the y-axis. A solid was formed from the revolution process and this represents the cylindrical tank solid. To create a fluid domain at the tank interior, a rectangular sketch with dimension 25.2 × 35 m was used. This dimension is lower than that used to create the outer cylinder. After generating the rectangular sketch, the sketch was then revolved 360° through the same axis to form a solid. The later will be assigned fluid properties to denote fluid domain or material. Last but not the least, a rectangular sketch of thickness 0.84 m was created and revolved 360° through the vertical axis to form the tank bottom support. These three (3) solids excluding the fluid domain was united using Boolean to form a single solid or fixed structure.

The next step was to dicretize the domain. The process of dividing the domain into smaller elements is termed meshing or griding. Various meshing strategy,

Table 1 Fluid material properties

Material Property	Consideration
Fluid type	LPG (propane) grade A
Molecular formula	C_3H_8
Density (compressible)	504 kg m^{-3}
Viscosity	0.58 cP
Fluid base temperature	28 °C
Molecular weight	44.09 kg $kmol^{-1}$
Specific heat capacity	1549 J kg^{-1} K^{-1}
Acentric factor	0.1521
Formation entropy	2.7014E + 05 J K^{-1}
Formation enthalpy	− 1.0386E + 08 J mol^{-1}
Isotropic thermal conductivity	0.0177 W m^{-1} k^{-1}

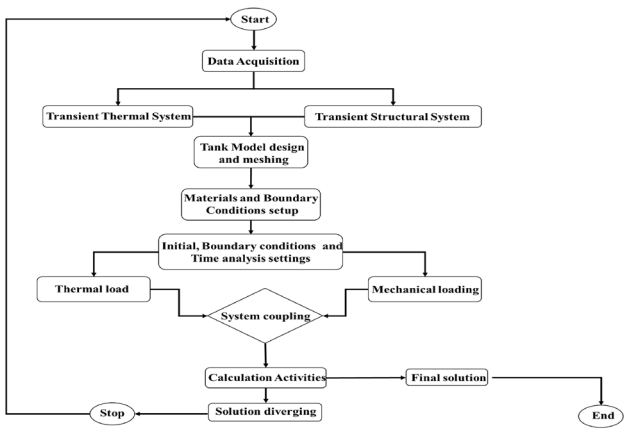

Fig. 1 simulation methodology flow chart

Table 2 stainless steel material properties

Material property	Consideration
Type	Stainless steel
Density	7750 kg m^{-3}
Isotropic property	Derived from young modulus
Young modulus	1.9E + 11 Pa
Bulk modulus	1.693E + 11 Pa
Poison ratio	0.31
Coefficient of thermal expansion	1.7E − 05 K^{-1}
Tensile yield strength	2.07E + 08 Pa
Compressive yield strength	2.07E + 08 Pa
Tensile ultimate strength	5.8E + 08 Pa

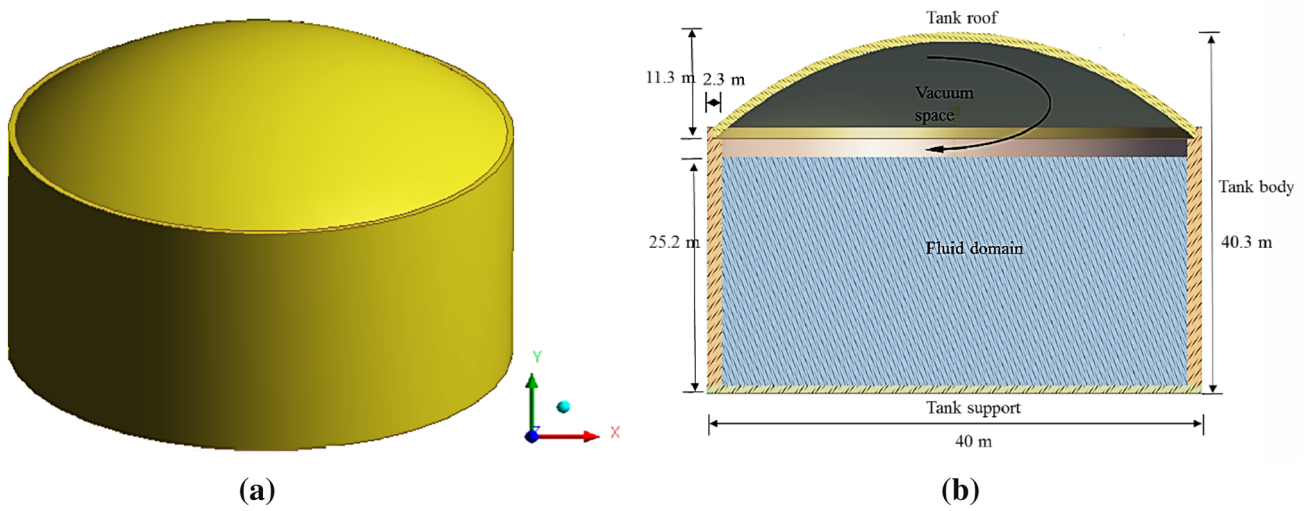

Fig. 2 **a** 3-D tank model geometry and **b** symmetric view of the geometry showing section dimensions

Table 3 tank model design considerations

Parameter	Dimension
Height of tank	40.3 m
Height of fluid	25.2 m
Tank diameter	40 m
Height of roof	11.3 m
Tank bottom thickness	0.9 m
Body Wall thickness	2.3 m
Roof wall thickness	1.4 m
Arc length	67.3 m
Tank surface area	32,178.6 m^2
Fluid volume	97,093.1 m^3
Tank interior volume	109,545.2 m^3

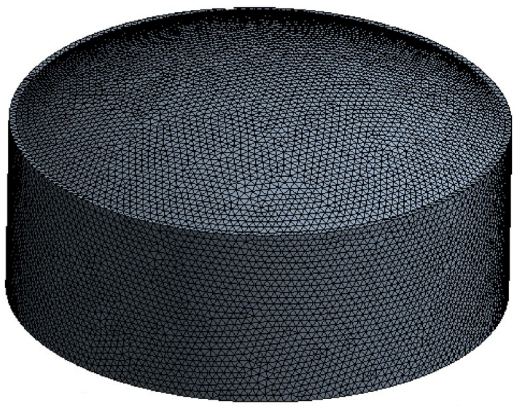

Fig. 3 Tank model mesh

their advantage and disadvantages have been extensively described in literature. The choice of meshing strategy is largely dependent on the complexity of the model geometric shape. Studies has shown that using an unstructured meshing is suitable for geometries with complex shape compared to using a structured meshing which is challenging to generate for such geometry type. With respect to the accuracy of the solver solution, using a structured meshing is preferable compared to the unstructured. In most cases, a hybrid meshing is used, and this approach requires higher computational time for the solver to converge to a solution and cost compared to the unstructured and structured meshing type. The meshing strategy employed in this study was the unstructured meshing using tetrahedrons. The model grid is shown in Fig. 3. The model grid is composed of 603,544 elements and 875,080 nodes. In addition, the element curvature angle was reduced to 4° with maximum element size of 1.2 m to generater a fine mesh. The meshing behaviour and algorithm used were soft and patch conforming method respectively. The physics preference was the non-linear mechanical APDL with element order controlled by the programme.

To ensure that the mesh settings are appropriate and could yield a reliable solution, a grid sensitivity study was conducted. From this analysis, it was observed that the predictions of Von Misses stress and elastic strain were changing with increasing number of elements. The body size was varied to increase the volume mesh density. At the end of this study, it was found that, the predictions converged after 300,000 elements. Therefore, the choice of most suitable mesh design was obtained within the convergence interval. The mesh sensitivity plot is shown in Fig. 4.

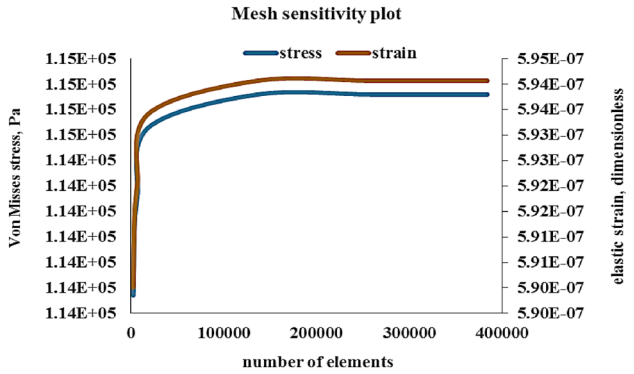

Fig. 4 Mesh sensitivity plot for Von Misses stress and elastic strain

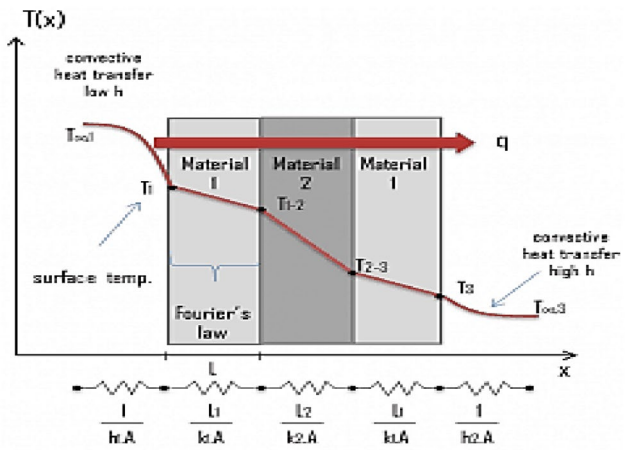

Fig. 5 Convective heat transfer process using the Fourier's law [10]

2.2 Heat transfer process modelling

Fundamentally, there exist three modes of heat transfer. That is heat transfer by conduction, convection and radiation. In some case, a combination of these could take place simultaneously [1]. In this paper, heat transfer by conduction and convection is expected to be experienced. The heat energy transferred to the fluid is sourced from the environment, such that, the tank structure conducts the heat and transfer the heat to the LPG by convection. In the process of heat transfer, heat is loss due to the material thermal resistance and thermal conductivity efficiency [1]. Heat flux, rate of heat transfer by conduction, wall thermal resistance and conductivity plays a significant role in the heat transfer process. It can be estimated from the Eqs. (2), (1), (3) and (4) respectively.

Heat transfer in a material is quantified using heat equations. Fundamentally, the Fourier law of thermal conduction is used to describe rate of heat transfer through a material by conduction. It is limited in application because, it assumes a steady state heat transfer [8]. This is not the case in real life scenarios. A major problem in heat conduction analysis is concerned with determining the temperature field in a particular medium resulting from the set boundary conditions during the analysis. The Fourier law is described mathematically as shown in the Eq. (1) below.

$$\overrightarrow{Q} = -k^{*}\nabla T \tag{1}$$

where $\overrightarrow{Q}$ is the local heat flux density along a specified direction, (W m^{-2}), k is the material conductivity (W k^{-1} m^{-1}) and ∇T is the temperature gradient (K m^{-1}).

The rate of heat transfer can easily be computed from the heat flux. This is by definition the rate of heat transfer per unit area. In most cases, it is referred to as heat flux density. With respect to the LPG tank structure, the heat flux is expected to be concentrated at areas in direct contact with the heat source. In this case, heat from the sun acts on the tank structure. The heat flux distribution can be estimated using the Eq. (2) below [8, 10].

$$q = \frac{Q}{A} \tag{2}$$

where A is the cross sectional area of heat transfer (m^2) and q is the heat flux (W m^2). The thermal conductivity and resistance on the tank wall can be calculated from the Eq. (3) and (4) below. The Fig. 5 below shows a typical example of heat low through a wall and its dependent variables, given that the thermal resistance of the materials, coefficient of thermal conductivity, wall area and boundary temperature is provided [8]. This figure is used to describe the heat transfer process from the environment through the tank wall, to the fluid.

The above described equations are applicable in the modeling of heat transfer interaction with the tank wall and exterior, provided that the wall thermal conductivity, resistance, temperature gradient, area and rate of heat loss is known [10].

Considering heat conduction in a large plane wall for which a uniform and constant heat is supplied per unit volume of the material, the thermal conductivity of the material can be derived from the partial differential heat equation below.

$$\frac{\partial^2 T}{\partial x^2} + \frac{q_v}{k} = 0 \tag{3a}$$

Solving the equation using indefinite integration, the general solution to the equation is;

$$T(x) = -\frac{q_v}{k}x^2 + C_1 x + C_2 \tag{3b}$$

where q_v is the rate at which heat energy is generated per unit volume of the material (LPG or stainless steel) (W m^{-3}),

C_1 and C_2 are the constant of integration, and T(x) is the temperature distribution (°C). With the case of the cylindrically shaped tank model, the heat transfer by conduction in the cylindrical coordinate best describe the thermal interaction. It can be modelled using the partial differential Eq. (3) below.

$$\frac{1}{r}\frac{\partial}{\partial r}\left(k \cdot r\frac{\partial T}{\partial r}\right) + \frac{1}{r^2}\frac{\partial}{\partial \emptyset}\left(k \cdot r\frac{\partial T}{\partial \emptyset}\right) + \frac{\partial}{\partial z}\left(k\frac{\partial T}{\partial z}\right) + q_v = \rho C_p \frac{\partial T}{\partial t} \tag{3c}$$

where ρ is the density of the material kg m^{-3} and C_p is the specific heat capacity of the material (J K^{-1} kg^{-1}).

For spherical coordinate,

$$\frac{1}{r^2}\frac{\partial}{\partial r}\left(k \cdot r^2\frac{\partial T}{\partial r}\right) + \frac{1}{r^2 \sin^2\theta}\frac{\partial}{\partial \emptyset}\left(k\frac{\partial T}{\partial \emptyset}\right) + \frac{1}{r^2 \sin^2\theta}\frac{\partial}{\partial \theta}\left(k \cdot \sin\theta\frac{\partial T}{\partial \theta}\right) + q_v = \rho C_p \frac{\partial T}{\partial t} \tag{3d}$$

Also, the thermal resistance of the material is obtained from the relation in Eq. (4) below.

$$Q = -kA\frac{T_2 - T_1}{L} = -\frac{T_2 - T_1}{R_t} \tag{4}$$

where Q is the heat flux through a plane (W), k is the conductivity of the material (W k^{-1} m^{-1}), L is the thickness of the material (stainless steel) (m) and A is the area through which heat is transferred into the system [10].

2.3 Boundary condition, solver preference and calculation activities

Setting up the boundary condition and physics is the next step of the simulation process. Proper implementation of the boundary temperature and pressure profile with time stepping is necessary. To identify potential regions with maximum stress concentrations under the action of extreme temperatures, the boundary temperature and pressure were set to range between – 20 to 30 °C and 25 to 30 GPa respectively for every 10 s, up to 100 s time steps. The relationship between the boundary temperature and pressure is shown in Fig. 6. The pressure was included as part of the boundary condition, because it is assumed that, at constant volume, the temperature of the material will vary proportionally to pressure. The gas laws confirm this theory. After identifying the stress hotspot, the boundary temperature extremity value was extended to cryogenic temperature so as to increase the temperature difference between the fluid environment and the exterior wall temperature. The total time steps was increased to 1,000,000 s with 20 sub-steps. In addition, the Fig. 7 below shows the boundary conditions and assignment. In the numerical simulation, the Mechanical APDL solver was used as the physics preference for the structural analysis.

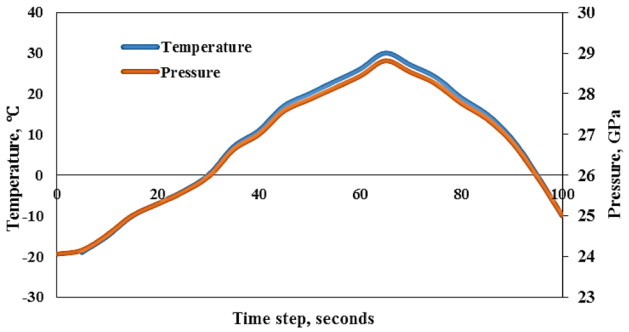

Fig. 6 Boundary temperature–pressure relationship with time steps

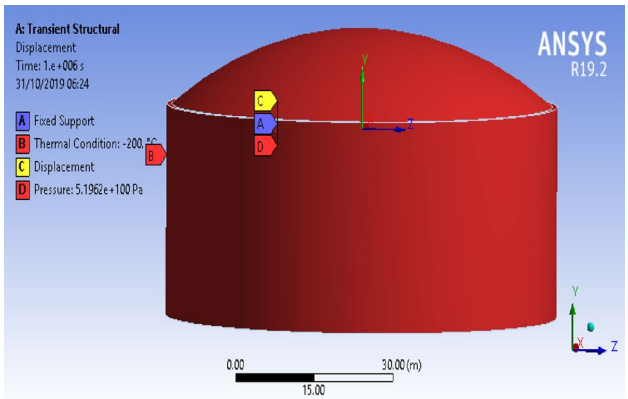

Fig. 7 Thermal and pressure load boundary assignment for the failure analysis

3 Results and discussion

3.1 Heat flux distribution

Heat flux distribution in space across the tank structure was modelled and simulated using the mathematical equations described in Sect. 2.2, Eq. (3). Figure 8a–c below shows the heat flux or change in temperature per unit area of the tank structure in the x-direction, y-direction and z-direction after 100 s time step respectively. From detailed look at Fig. 8, it was observed that the heat flux intensity was pronounced along the vertical axis, were the tank roof directly contacts or receives the heat energy from the sun rays, compared to other parts of the structure. It is expected that stress due to an increasing temperature gradient will be concentrated at this region.

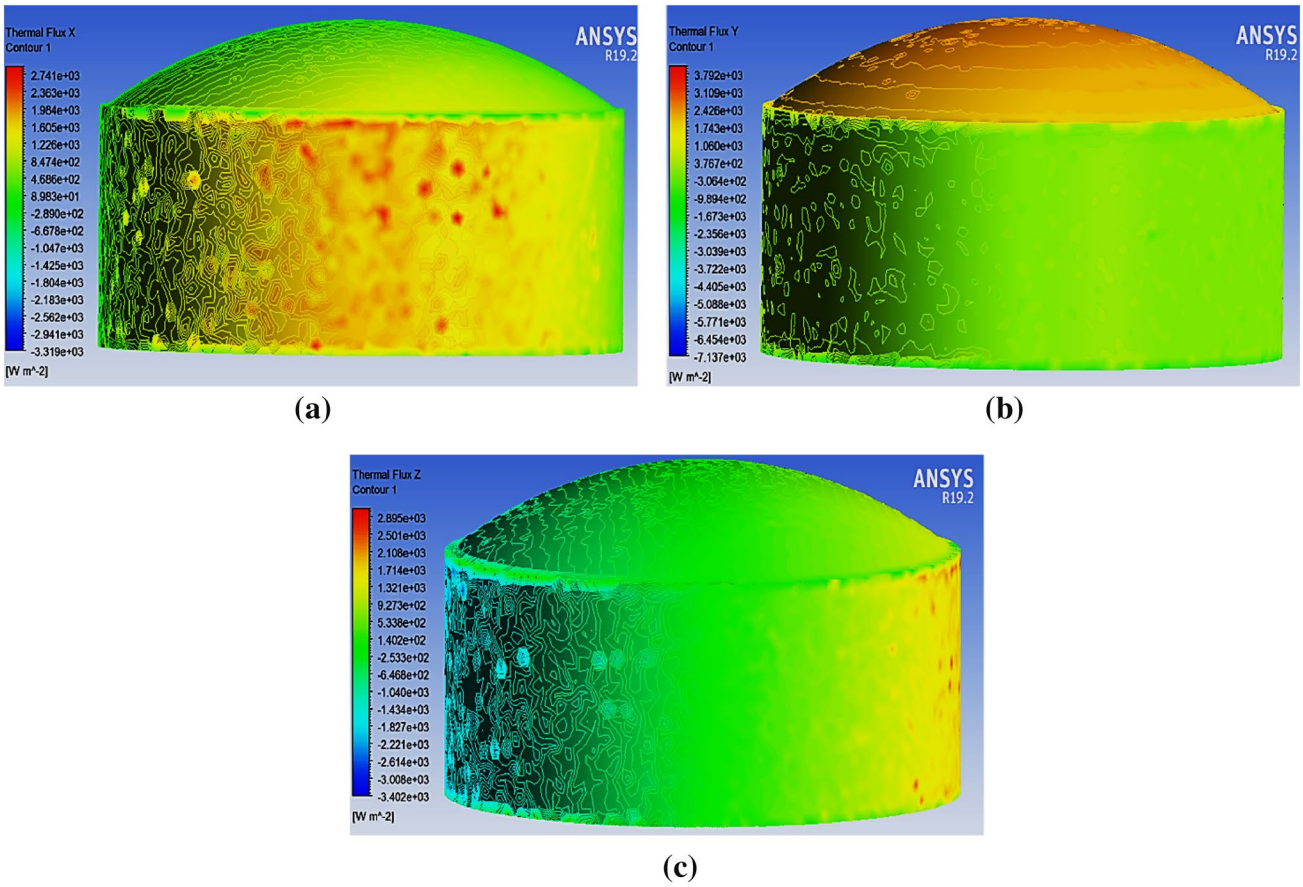

Fig. 8 Heat flux distribution in the **a** x-direction, **b** y-direction and (c) z-direction

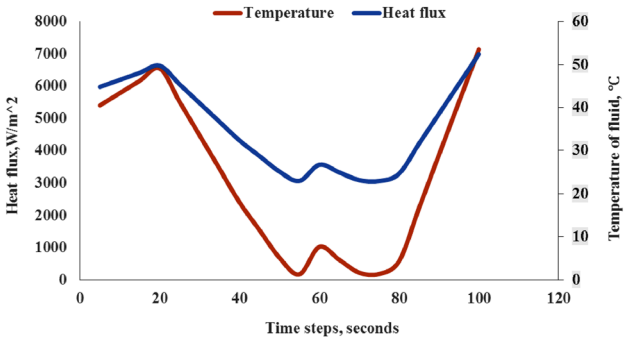

Fig. 9 Rate of heat flux with temperature change

The plot in Fig. 8 below describes the relationship between temperature, heat flux and time. Be informed that the heat flux or concentration is a function of temperature gradient and the tank wall thickness computed using the Eqs. (1) and (2) in Sect. 2.2. Notice that from the highlighted model equations, the heat flux is directly proportional to the temperature. Comparing this with the plot shown in Fig. 8 below, both profiles correlated proportionally to each other, and hence confirms proper implementation of the heat equations.

The plot shown in the Fig. 9 below was obtained from collecting the maximum heat flux and temperature values about the tank material for every 10 s. It depicts that the heat distribution is non-linearly related with time and could induce a sharp rise in temperature gradient on the material. The resultant effect of these is the generation of thermal stress at areas experiencing increased rate of temperature change.

3.2 Fluid material deformation

LPG is a type of fluid that that vividly response to a change in the temperature gradient due to its thermodynamic properties. One of this property is its ability to volatilize at lower vapour pressure, conventionally below 2.206 GPa. At this critical point, the fluid begins to observe a non-linear behaviour with respect to the phase formed and displacement of the gas molecules. Detail knowledge about the behaviour of the gas/liquid molecules under the influence of absorbed thermal energy can properly be investigated from fluid molecular dynamics analysis (FMDA). This is not the focus of this paper.

The response or motion of the fluids can also be evaluated from fluid mechanics point of view. In this case, the elastic and shear strain are used. Strain is the ratio of the deformed length to the original shape of the fluid bulk at a particular instance. The image show in Fig. 10a, b respectively describes the equivalent elastic strain and strain due to shear between the deformed fluid interfaces. The figure was post-processed at the end of 100 s time step.

It depicts that the bulk is deformed in an unsteady manner as a result of the uneven heat transfer distribution from the exterior, through the Fluid-wall interface and to the fluid. It was observed that the strain was concentrated at extreme points, than at the centre. This can be accounted from the shape of tank model at the bottom support and roof intersect. The resultant effect of the fluid strain or deformation exerts some amount of stress to the container wall adding to that exerted by the surrounding or boundary conditions. This is further discussed in Sect. 3.4.

3.3 Von Misses stress intensity analysis

Stress acting on a material leading to deformation can be evaluated using the Von Misses stress intensity. From previous discussion, it was deduced that stress is being exerted on the tank surface as a result of the fluid strain and boundary conditions. From design point of view, petroleum products container or storage vessels are designed to better manage pressure and prevent stress concentration

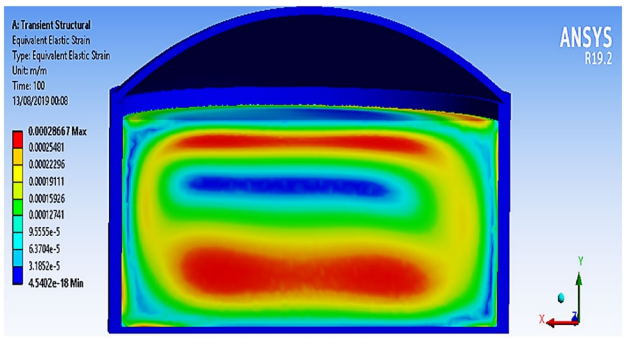

Fig. 10 Equivalent elastic and shear elastic strain for the fluid bulk

at a point. Most LPG tanks are spherical in shape, whiles others are cylindrical in shape. The key difference lies on the concept that, in some refineries or gas processing plant for example the Atuabo Gas Processing Plant (AGPP) in Ghana, the LPG tanks are made spherical because external pressure is required to maintain the gas in the liquid state. This is not the case for vertical or cylindrical LPG tanks were the gas is first liquefied and stored. This represents the key reason why some petroleum refineries decides to store LPG in vertical tanks or spherical tanks. Comparing both designs, the spherical shaped LPG tanks are known to manage pressure better than the cylindrical counterpart. Pressure management of the vessel with respect to their structure, relies greatly on the structure's shape.

From observation of Fig. 11, it was obvious that the stress distribution is not even across the structure surface for different time consideration. Recall that the temperature at the boundary condition was made to increase from −20 to 30 °C after 60 s and then drops from 30 to −15 °C at the end of 100 s. This boundary setting was made so for analytic purpose, to aid achievement of the research goal. Notwithstanding, the fluid temperature was kept constant at 28 °C.

The stress intensity was pronounced at the initial stage and final time step were the temperature gradient was maximum. Results shown in Fig. 11 depicts that the stress is concentrated at the principal plane were that tank roof is connected to the cylindrical structure. This confirms the hypothesis made in Sect. 2.1 of this paper. From an extensive search of the literature, it proven that stress is concentrated at sharp points, and this was the case for the tank structure used in this investigation shown in Fig. 11. The maximum stress value achieved at this stage was 3.554×10^3 Pa. This value is below the yield point of the material (205 GPa) and hence, the material is not expected to fail at the thermal and mechanical condition. Therefore, this calls for a failure analysis. In addition, the Fig. 12 below shows the stress and strain relationship with time. It can be observed that the stress and strain values reduced with time and temperature gradient.

The sharp points with high stress concentration represents the potential are on the tank structure exposed to deformation or failure at an extended period of time [6]. Recall that, the transients thermal and structure system were coupled to evaluate the effect of thermal loads on the structure integrity in terms of deformation or failure.

3.4 Failure analysis and model validation

The stress–strain curve for the stainless steel material shown in Fig. 13 describes the fracture strength of the material under the prescribed boundary condition. It is obvious that the material will fail at an elevated temperature cited in Sect. 1. The fatigue failure was most likely to originate from crack at an inclusion in the grain boundary of the

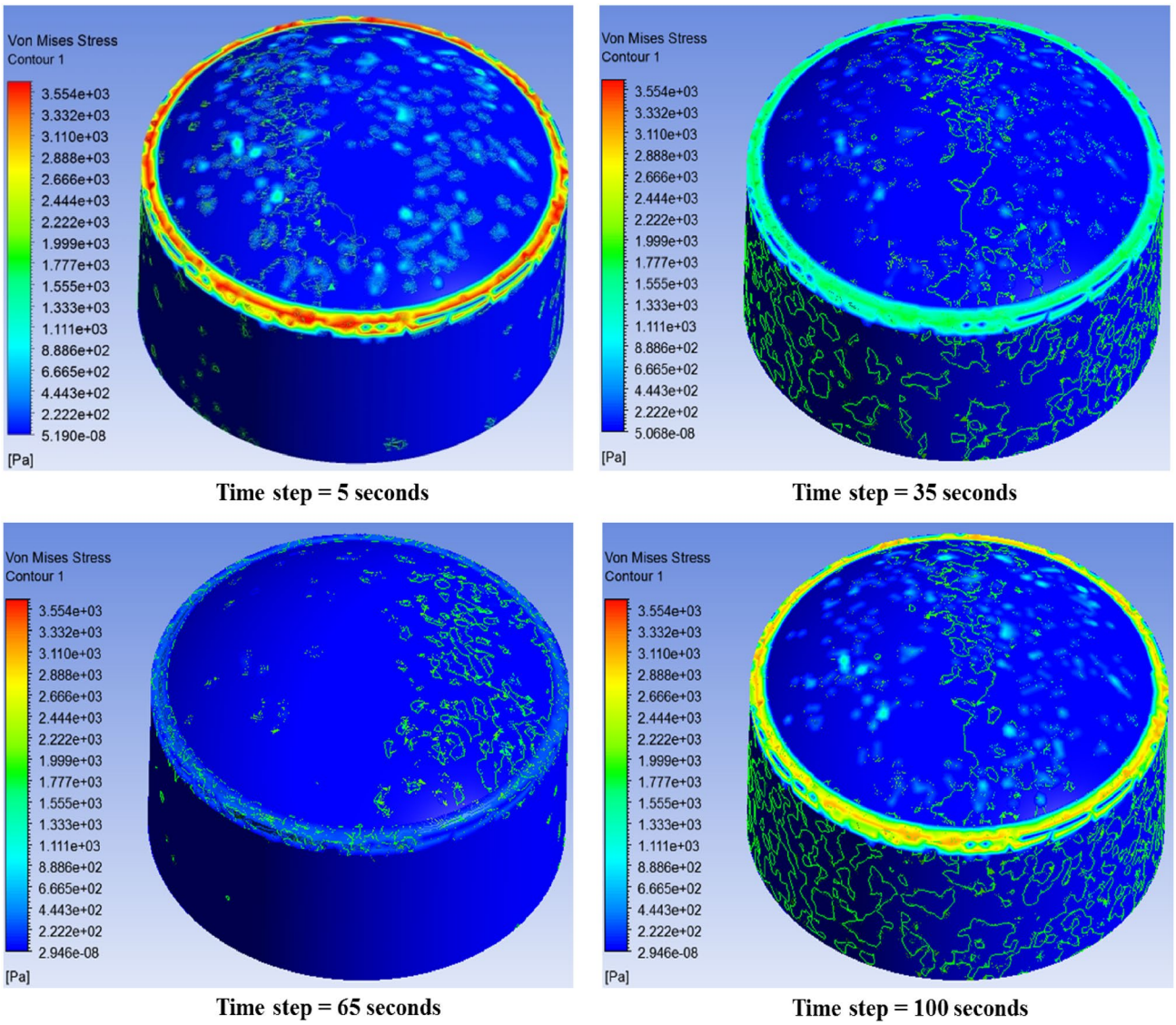

Fig. 11 Stress intensity distribution with time steps

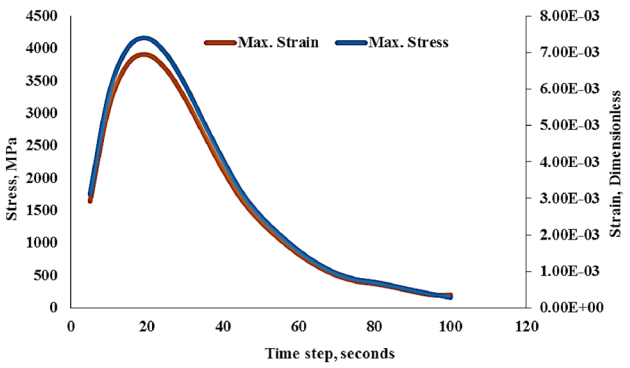

Fig. 12 Stress and strain relationship versus time steps in seconds

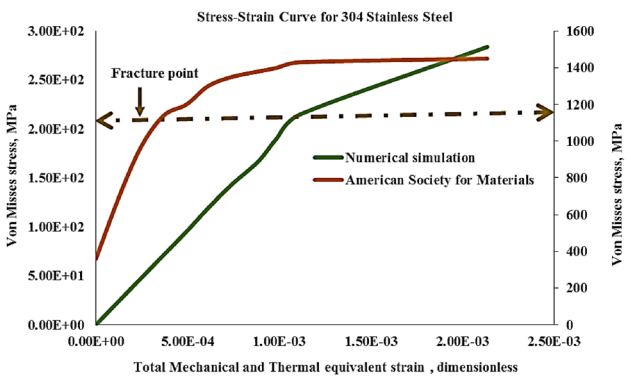

Fig. 13 Stress–strain curve demonstrating failure of the stainless steel material

austenitic microstructure [14, 18]. Here, the action of heat degrades the grains which constitutes the structure and hence reduces the connective strength of the microstructure. These results to a reduced stiffness of the stainless steel material. The stiffness of a material is determined from the slope of the stress–strain curve within the elastic limit [19].

The results obtained from the numerical simulation was validated with a typical stress–strain plot for 304 stainless steel material. Both plot are observed to profile fairly well and the fracture point identified with a dash line are well aligned. Comparing both plot, the material is seen to have fractured at a lower stress value of about 210 MPa. This can be explained from the point of view that extreme thermal and mechanical loads were exerted on the material for a prolong simulation period of 1,000,000 s. As discussed earlier these forces induces fatigue and disrupts the microstructure of the material and therefore reduces the resistance of the material to fracture.

4 Conclusion

Findings from this study depicts that temperature has a direct impact on the stiffness of stainless steel materials. It showed that, the higher the intensity of the thermal load, the greater the stress experienced on the material at local points. However, using a different approach compared to literature yielded similar output. The principal plane connecting the model design roof to the cylindrical structure was identified to be the possible area exposed to maximum stress concentration and eventually fatigue failure of the austenitic material. From the failure analysis, stiffness was found to decrease with increasing temperature gradient and mechanical load.

Acknowledgement We want to acknowledge GOD for the Grace and knowledge imparted on us and All Nations University College, Ghana for providing the platform to successfully complete this research.

Compliance with ethical standards

Conflict of interest The authors declare that they have no conflict of interest.

References

1. Abbasi FM, Shehzad SA (2016) Heat transfer analysis for three-dimensional flow of Maxwell fluid with temperature dependent thermal conductivity: application of Cattaneo–Christov heat flux model. J Mol Liq 220:848–854
2. Abendroth M, Kuna M (2003) Determination of deformation and failure properties of ductile materials by means of the small punch test and neural networks. Comput Mater Sci 28(3–4):633–644
3. Adnyana DN (2018) Failure analysis of stainless steel heat exchanger tubes in a petrochemical plant. J Fail Anal Prev 18(2):413–422
4. Afshan S, Francis P, Baddoo NR, Gardner L (2015) Reliability analysis of structural stainless steel design provisions. J Constr Steel Res 114:293–304
5. DiGiovanni C, Li L, Driver R, Callele L (2017) Cracking in welded steel platform structures during hot-dip galvanization. Eng Fail Anal 79:1031–1042
6. Ercolino M, Magliulo G, Manfredi G (2016) Failure of a precast RC building due to Emilia-Romagna earthquakes. Eng Struct 118:262–273
7. Fuller RW, Ehrgott JQ Jr, Heard WF, Robert SD, Stinson RD, Solanki K, Horstemeyer MF (2008) Failure analysis of AISI 304 stainless steel shaft. Eng Fail Anal 15(7):835–846
8. Han JC (2016) Analytical heat transfer. CRC Press, Boca Raton
9. Idapalapati S, Loh KK, Yeo S (2017) Failure investigation of welded high nickel stainless steel flange-elbow joint. Eng Fail Anal 78:99–109
10. Kakaç S, Yener Y, Naveira-Cotta CP (2018) Heat conduction. CRC Press, Boca Raton
11. Kumar MS, Sujata M, Venkataswamy MA, Bhaumik SK (2008) Failure analysis of a stainless steel pipeline. Eng Fail Anal 15(5):497–504
12. Maharaj C, Marquez A (2019) Failure analysis of a stainless steel pipe elbow in a purge gas line. J Fail Anal Prev 19(1):15–23
13. Mubarok N, Notonegoro HA, Thosin KAZ (2018) Comparative mechanical improvement of stainless steel 304 through three methods. In: IOP conference series: materials science and engineering, vol 367, No 1, p 012023. IOP Publishing
14. Pham HT, Iwamoto T (2017) A computational investigation on small punch test for evaluating fracture toughness of TRIP steel at higher deformation rate. In: Key engineering materials. vol 725, pp 66–71. Trans Tech Publications
15. Reinders JEA, Velthuis JFM, Spruijt MPN (2019) Pressure and temperature increase of LPG in a thermally coated pressure vessel exposed to fire: experimental and model results. J Loss Prev Process Ind 57:55–60
16. Scarponi GE, Landucci G, Heymes F, Cozzani V (2018) Experimental and numerical study of the behavior of LPG tanks exposed to wildland fires. Process Saf Environ Prot 114:251–270
17. Shi GH, Aye L, Liu YC, Du XJ (2018) Dynamic simulation of liquefied petroleum gas vaporisation for burners. Appl Therm Eng 137:575–583
18. Van Do VN, Lee CH, Chang KH (2015) High cycle fatigue analysis in presence of residual stresses by using a continuum damage mechanics model. Int J Fatigue 70:51–62
19. Weck R (1965) Failure of steel structures: causes and remedies. Proc R Soc Lond A 285(1400):3–9